Extending Darcy's law to the flow of yield stress fluids in packed beds: method and experiments

Antonio Rodríguez de Castro[a,b]

[a] Arts et Métiers ParisTech, Rue Saint-Dominique, 51006 Châlons-en-Champagne, France
[b] Laboratoire MSMP-EA7350, Rue Saint Dominique, 51006 Châlons-en-Champagne, France

A B S T R A C T

A large number of complex fluids commonly used in industry exhibit yield stress, e.g., concentrated polymer solutions, waxy crude oils, emulsions, colloid suspensions and foams. Yield stress fluids are frequently injected through unconsolidated porous media in many fields such as soil remediation and reservoir engineering, so modelling their flow through this type of media is of great economic importance. However, obtaining macroscopic laws to model non-Newtonian flow poses a considerable challenge given the dependence of the viscosity of the fluid on pore velocity. For this reason, no macroscopic equation is currently available to predict the relationship between injection flow rate and the pressure drop generated during the flow of a yield stress fluid without using any adjustable parameter. In this work, a method to extend Darcy's equation to the flow of yield stress fluids through model unconsolidated porous media consisting of packs of spherical beads is presented. Then, the method is experimentally validated through comparison with a total of 572 experimental measurements obtained during the flow of a concentrated aqueous polymer solution through different packs of glass spheres with uniform size. An improved prediction of the pressure drop-flow rate relationship is achieved by taking into account the non-linear relationship between apparent shear rate and average pore velocity.

1. Introduction

The flow of complex fluids in unconsolidated porous media is involved in many economically important industrial applications, e.g., remediation of polluted soils (Gastone et al., 2014), Enhanced Oil Recovery (EOR) (Wang et al., 2017), rock fracturing (Roustaei et al., 2016) and liquid food engineering (Welti-Chanes et al., 2005). Numerous complex fluids are shear-thinning, showing a decrease in shear viscosity as the applied shear rate is increased. Shear-thinning fluids are extensively used in petroleum engineering and soil remediation to improve the microscopic sweep of the reservoir through stabilization of the injection front (Lake, 1989; Silva et al., 2012; Wever et al., 2011). In some cases, fluids with shear-rate dependent viscosity additionally present a yield stress, i.e., a threshold value in terms of shear stress below which they do not flow. In the specific field of petroleum engineering, the drilling fluids injected into rocks for the drilling of wells are often designed so as to have a yield stress in order to prevent cutting from settling when circulation stops (Lavrov, 2013; Coussot, 2014). Some examples of yield stress fluids used in oil industry include emulsions, drilling muds, polymeric gels such as Carbopol, hevy oils and foams (Talon et al., 2014). Furthermore, a number of fracturing fluids used in hydraulic fracturing as gelling agents exhibit a yield stress designed to enhance proppant transport (Roustaei et al., 2016). Among them, guar, hydroxypropyl guar, carboxymethyl hydroxypropyl guar, hydroxyethyl cellulose, and polyacrylamide are of particular relevance (Belyadi et al., 2016).

Predicting the pressure drop of a yield stress fluid flowing through unconsolidated porous media is especially important, given that a great number of petroleum reservoirs are located in unconsolidated formations (Peng et al., 2007; Pang and Liu, 2013). The majority of laboratory experiments in this field have been performed using beds of spherical beads, which represent an idealization of unconsolidated porous media (Rao and Chhabra, 1993; Tiu et al., 1997; Basu, 2001). The Newtonian case is generally well understood in this type of porous media and allows process design calculations with acceptable levels of accuracy. The extensive literature regarding the flow of fluids with complex rheology through unconsolidated packed beds was critically reviewed by Chhabra et al. (2001), and Sochi (2010) analysed the available models for describing non-Newtonian single-phase flow in porous media. More recently, Rodríguez de Castro and Radilla (2017a) extended Forchheimer's law and Ergun's equation to the flow of fluids with shear-rate-dependent viscosity through packs of glass spheres with uniform size. The latter authors determined the accuracy of the extended laws under creeping and inertial regimes from comparison with a full set of experiments. Nevertheless, the yield stress effect was not addressed in the preceding works and obtaining a macroscopic law for the flow of yield stress fluids has proved to be a stumbling-block.

Talon and Bauer (2013) performed Lattice-Boltzmann simulations to solve 2D flow of Bingham yield stress fluids in porous media, and distinguished three different flow regimes. These regimes corresponded to 1) the flow of a single pore, 2) progressive pores opening and 3) flow of all pores. Furthermore, Chevalier et al. (2013) focused on obtaining a generic relationship between flow rate and pressure drop applicable to the Darcian flow of yield stress fluids through packed beds. These authors proposed a macroscopic equation in which only the parameters of

E-mail address: antonio.rodriguezdecastro@ensam.eu

https://doi.org/10.1016/j.advwatres.2019.01.012

the rheological law of the injected fluid, the diameter of the beads and two coefficients related to the internal structure of the porous medium were used as inputs. Then, Chevalier et al. (2014) conducted NMR experiments which contributed to elucidate the structural parameters appearing in this generic law. However, the determination of these coefficients is still unclear and the proposed formula presents the inconvenient of assuming linear relationship between shear rate and Darcy velocity in definition of the apparent shear rate in the porous medium. Moreover, the extension of Darcy's equation to the flow of yield stress fluids proposed by Chevalier et al. (2013) still has to be confirmed by further laboratory experiments given the serious lack of reliable experimental data in the literature (Lavrov, 2013; Coussot, 2014).

Inspired by the broad interest of extending Darcy's law to the flow of yield stress fluids through model unconsolidated porous media, the objective of this work is to provide a straightforward procedure to predict the relationship between pressure gradient and flow rate. The proposed method is also evaluated through comparison with experimental data. To do so, a series of flow experiments through four different packs of mono-size spherical glass beads were carried out using concentrated aqueous solutions of xanthan biopolymer presenting a yield stress. The effect of beads size on the accuracy of the predictions is then assessed and discussed.

In the area of non-Newtonian flow in porous media, still very open, it is crucial to base the interpretations and the modelling on solid observations. The experimental details concerning the injection of xanthan gum solutions in different types of porous media have been carefully evaluated and discussed in the past: Rodríguez de Castro (2014), Rodríguez de Castro et al. (2014, 2016, 2018), Rodríguez de Castro and Radilla (2017b). In all these preceding works, the same aqueous polymer solution was used and the experimental aspects were thoroughly addressed, including a discussion on the rheological model, the existence of a plateau viscosity, the capability of the fluid to emulate yield stress behaviour and the interactions between fluid and porous medium (polymer retention, mechanical degradation and polymer adsorption). For this reason, it was decided in the present work to capitalize the knowledge acquired from the preceding research by using the same extensively investigated xanthan gum solution.

2. Predicting the flow of yield stress fluids in packed beds

2.1. Previous attempts to extend Darcy's law to the flow of yield stress fluids

Herschel-Bulkley empirical law (Herschel and Bulkley, 1926) is commonly used to describe the rheological behaviour under shear of a large group of time-independent yield stress fluids. This law can be written as follows:

$$\begin{cases} \tau = \tau_0 + a\dot{\gamma}^n \text{ for } \tau > \tau_0 \\ \dot{\gamma} = 0 \text{ for } \tau \leq \tau_0 \end{cases} \quad (1)$$

where τ is the shear stress experienced by the fluid at a given shear rate $\dot{\gamma}$, τ_0 is the yield stress, a is the consistency and n is the flow index of the fluid. In the case of shear-thinning yield stress fluids, n is inferior to unity. The three parameters are generally obtained by fitting the data obtained by measuring the shear rate $\dot{\gamma}$ as a function of the applied shear stress τ with a rheometer.

Several attempts have been made to obtain a macroscopic law linking the injection flow rate to the resulting pressure drop during the flow of yield stress fluids in porous media (Pascal, 1981; Pascal, 1983; Al-Fariss and Pinder, 1987; Chase and Dachavijit, 2005; Coussot, 2014). Pascal modified Darcy's law by introducing a threshold pressure gradient ∇P_t to account for the yield-stress (Pascal, 1981): $\nabla P_t = \frac{\varphi \tau_0}{\sqrt{K}}$. ∇P_t is directly proportional to τ_0 and inversely proportional to the square root of the absolute permeability K. However, Pascal's relationship presents the serios drawback of including a dimensionless constant φ that must be empirically determined for each fluid-medium pair. Also, it only applies to the case $n=1$. Indeed, the existence of experimentally adjustable parameters with no clear physical meaning as inputs, which impedes direct computational predictions, is a major drawback of most available macroscopic flow expressions. In this regard, Shahsavari and McKinley (2016) conducted numerical simulations providing analytical expressions for such parameters in the particular case of fibrous materials, without including any specific dependence of these coefficients on the injection velocity. Only a few experimental works exist for the flow of yield stress fluids in porous media (Al-Fariss and Pinder, 1987; Chase and Dachavijit, 2005; Chevalier et al., 2013; Chevalier et al., 2014; Rodríguez de Castro, 2016), and the ranges of variation of the flow rate are usually narrow. These experimental works showed that the relationship between the absolute value of the pressure gradient ∇P and the absolute value of Darcy velocity u is of the same form as the constitutive equation of the fluid, i.e. $\nabla P = \nabla P_t + Cu^n$ with C being a parameter that depends on the porous medium and the boundary conditions.

More recently, Chevalier et al. (2013) presented a simple approach to extend Darcy's law to the flow of yield stress fluids. This general law contains a yielding term which may be simply expressed as a function of the yield stress of the material and the bead size:

$$\nabla P = \frac{\chi \tau_0}{d_s} + \frac{\omega a \left(\frac{u}{d_s}\right)^n}{d_s} \quad (2)$$

with ΔP being the absolute value of the pressure drop through the packed bed of length L, $\nabla P = \frac{\Delta P}{L}$ the magnitude of the pressure gradient, Q the volume flow rate, A the cross-sectional area, $u = Q/A$ the absolute value of the Darcy velocity and d_s the diameter of the spherical beads. The latter authors initially stated that χ and ω in Eq. (2), should be universal factors for the flow through spherical beads. The first coefficient is related to the path of maximum width throughout the porous medium while the second coefficient reflects the pore size distribution. However, on the basis of the results obtained by NMR measurements, it was subsequently shown that χ and ω are two dimensionless coefficients depending only on the distribution of shear rate intensity and on the coefficient n, which are in turn fluid-dependent (Chevalier et al., 2014). Also, u/d_s was considered to be the apparent shear rate for the flow through such a porous medium, which is a serious flaw of Eq. (2). Indeed, the apparent shear rate was shown not be proportional to u in the case of yield stress fluids flowing at low and moderate flow rates (Rodríguez de Castro and Radilla, 2017b).

The first (yielding) term on the right hand side of Eq. (2) corresponds to the critical pressure gradient below which no flow occurs. The second term is velocity-dependent, and expresses the additional viscous pressure drop above the yielding pressure once the fluid is flowing. Chevalier et al. (2013) experimentally determined the values of χ and ω, obtaining $\chi = 12$ for a Carbopol aqueous solution and $\chi = 5.5$ for a water-in-oil emulsion, which did not permit to validate the universality of this coefficient. In contrast, these authors found that $\omega = 85$ for both types of fluids.

2.2. New approach to extend Darcy's law to the flow of yield stress fluids

As mentioned above, despite the method presented by Chevalier et al. (2013) being a valid approach, the choice of d_s as characteristic length in the definition of the apparent shear rate and the non-dependence on injection velocity remain debatable. Also, the values of χ and ω are not easily predictable. For these reasons, the objective of this subsection is to present a method to simply predict the u vs. ∇P relation by properly defining the actual shear rate and the shear viscosity of the fluid in the porous medium.

Darcy's law (Darcy, 1856) describes the single-phase flow of incompressible Newtonian fluids through porous media at low values of Reynolds number:

$$\nabla P = \frac{\mu}{K}\frac{Q}{A} = \frac{\mu}{K}u \quad (3)$$

where μ is the shear viscosity of the injected fluid, and K is the intrinsic permeability. Moreover, Kozeny-Carman equation allows to predict K from the porosity ε of the bed and the diameter of the beads using hydraulic radius theory:

$$K = \frac{\varepsilon^3 d_s^2}{36\kappa(1-\varepsilon)^2} \tag{4}$$

κ being the Kozeny-Carman constant, the value of which is generally set to $\kappa = 5$ in packs of spheres (Kaviany, 1995).

Previous works have shown that some concentrated polymer solutions are yield stress fluids (Song et al., 2006; Carnali, 1991; Withcomb and Macosko, 1978; Economides and Nolte, 2000; Khodja, 2008; Benmouffok-Benbelkacem et al., 2010). The steady-state shear flow of these solutions can be well described by the Herschel-Bulkley law (Eq. (1)). A practical approach to study the flow of complex fluids through a porous medium consists in defining an equivalent viscosity μ_{eq} as being the quantity that must replace the viscosity in Darcy's law to result in the same pressure drop actually measured (Tosco et al., 2013):

$$\mu_{eq} = K\frac{\nabla P}{u} \tag{5}$$

In order to predict μ_{eq} from the constitutive equation of the fluid, an apparent shear rate in the porous medium $\dot{\gamma}_{pm}$ has to be determined first. Assuming a bundle-of-capillaries model $\dot{\gamma}_{pm}$ is usually taken as four times the average pore velocity $4\,u/\varepsilon$ divided by the average pore throat radius $\bar{r}$ (characteristic length of the microscopic flow) (Chauveteau and Zaitoun, 1981; Chauveteau, 1982; Sheng, 2011). $\bar{r}$ can be estimated from the permeability K and the porosity ε of the porous medium, as proposed by Kozeny (1927) using a bundle-of-capillaries model:

$$\bar{r} = \sqrt{\frac{8K}{\varepsilon}} \tag{6}$$

According to the preceding definition, $\dot{\gamma}_{pm}$ can be expressed as:

$$\dot{\gamma}_{pm} = \frac{4\alpha\frac{u}{\varepsilon}}{\bar{r}} = \alpha\frac{\sqrt{2}u}{\sqrt{K\varepsilon}} \tag{7}$$

where α is an empirical shift factor known to be a function of both the bulk rheology of the fluid and the tortuosity of the packed bed (Chauveteau, 1982; Sorbie et al., 1989; López et al., 2003; López, 2004; Comba et al., 2011). Therefore, $\dot{\gamma}_{pm}$ corresponds to the wall shear rate in a pore section of radius $\bar{r}$. This definition of apparent shear rate is in contrast with the one used by Chevalier et al. (2013), in which d_s is taken as characteristic length instead of $\frac{\sqrt{K\varepsilon}}{\sqrt{2}}$. For the creeping flow of Herschel-Bulkley fluids, μ_{eq} can be obtained from Eqs. (1) and (7):

$$\mu_{eq} = \frac{\tau_0\sqrt{K\varepsilon}}{\alpha\sqrt{2}u} + a\left(\alpha\frac{\sqrt{2}u}{\sqrt{K\varepsilon}}\right)^{n-1} \tag{8}$$

Keeping in mind the objective to propose a prediction method, analytical expressions for the calculation of α must be provided. In order to obtain such expressions, let us focus now on the determination of the wall shear rate in circular channels. For the steady flow of an incompressible fluid through a circular channel of radius $\bar{r}$, the wall shear stress τ_w is related to the pressure gradient ∇P as follows:

$$\tau_w = \frac{\nabla P\bar{r}}{2} \tag{9}$$

Using Eqs. (3) , (8), (9) can be written as:

$$\tau_w = \left(\frac{\tau_0}{\dot{\gamma}_{pm}} + a\dot{\gamma}_{pm}^{n-1}\right)\frac{u}{K}\frac{\bar{r}}{2} = \frac{1}{2\sqrt{2}}\sqrt{\frac{\varepsilon}{K}}\frac{\bar{r}}{\alpha}\tau_0 + \frac{2^{\frac{n-3}{2}}}{K^{\frac{n+1}{2}}\varepsilon^{\frac{n-1}{2}}}\frac{\bar{r}}{\alpha^{1-n}}au^n \tag{10}$$

For a constant viscosity incompressible fluid, the wall shear rate $\dot{\gamma}_{w,Newtonian}$ is given by $\dot{\gamma}_{w,Newtonian} = \alpha_N\frac{4\frac{u}{\varepsilon}}{\bar{r}}$, where α_N is the shift factor for the injection of a Newtonian fluid. α_N is related to the tortuosity of the fluid flow through the packed bed and its value was shown to be 0.69 for spherical beads (Christopher and Middleman, 1965; Shenoy, 1994). However, this value $\alpha_N = 0.69$ has been contested by some authors (James and McLaren, 1975; Chaveteau, 1982). For this reason, in this work α_N will be considered first as unknown and will be determined through fitting to the experimental u vs. ∇P data. Then, the obtained α_N will be compared to the values previously reported in the literature.

The wall shear rate for the flow of liquids with a shear-rate-dependent viscosity can be calculated by using the Weissenberg-Rabinowitsch-Mooney equation (Rabinowitsch, 1929; Mooney, 1931):

$$\begin{aligned}\dot{\gamma}_{pm} &= \frac{\dot{\gamma}_{w,Newtonian}}{3}\left[2 + \frac{\mathrm{d}\left(\ln\dot{\gamma}_{w,Newtonian}\right)}{\mathrm{d}\left(\ln\tau_w\right)}\right] \\ &= \frac{\dot{\gamma}_{w,Newtonian}}{3}\left[2 + \frac{\frac{\mathrm{d}\left(\ln\dot{\gamma}_{w,Newtonian}\right)}{\mathrm{d}u}\mathrm{d}u}{\frac{\partial\left(\ln\tau_w\right)}{\partial u}\mathrm{d}u + \frac{\partial\left(\ln\tau_w\right)}{\partial\alpha}\mathrm{d}\alpha}\right] \\ &= \frac{\dot{\gamma}_{w,Newtonian}}{3}\left[2 + \frac{\frac{\mathrm{d}\left(\ln\dot{\gamma}_{w,Newtonian}\right)}{\mathrm{d}u}}{\frac{\partial\left(\ln\tau_w\right)}{\partial u} + \frac{\partial\left(\ln\tau_w\right)}{\partial\alpha}\frac{\mathrm{d}\alpha}{\mathrm{d}u}}\right]\end{aligned} \tag{11}$$

where α is a function of u. Weissenberg-Rabinowitsch-Mooney equation is commonly used to calculate the wall shear rate of complex fluids with non-parabolic velocity profiles, including yield stress fluids (Macosko, 1994; Steffe, 1996; Pipe et al., 2008; Sochi, 2015). The following assumptions are used in the derivation of Eq. (11): incompressible fluid, steady state, laminar flow regime, no wall-slip, no end-effects, unidirectional flow, temperature is constant and properties are not a function of time or pressure (Steffe, 1996).

For a Herschel-Bulkley fluid, Eq. (11) becomes:

$$\dot{\gamma}_{pm} = \frac{\alpha_N}{\bar{r}}\frac{4u}{3\varepsilon}\left(2 + \frac{\alpha\left(\tau_0 + 2^{\frac{n}{2}}a\left(\alpha\frac{u}{\sqrt{K\varepsilon}}\right)^n\right)}{2^{\frac{n}{2}}an\alpha\left(\alpha\frac{u}{\sqrt{K\varepsilon}}\right)^n - 2u\left(\tau_0 - 2^{\frac{n}{2}}a(n-1)\left(\alpha\frac{u}{\sqrt{K\varepsilon}}\right)^n\right)\frac{\partial\alpha}{\partial u}}\right) \tag{12}$$

From Eq. (12), it can be deduced that α becomes the constant value $\alpha^* = \frac{\alpha_N}{3}(2+\frac{1}{n})$ for very high values of u. By combining Eqs. (7) and (12), the following differential equation is obtained, which allows the determination of α as a function of u:

$$\alpha = \frac{\alpha_N}{\bar{r}}\frac{2\sqrt{2}\sqrt{K}}{3\sqrt{\varepsilon}}\left(2 + \frac{\alpha\left(\tau_0 + 2^{\frac{n}{2}}a\left(\alpha\frac{u}{\sqrt{K\varepsilon}}\right)^n\right)}{2^{\frac{n}{2}}an\alpha\left(\alpha\frac{u}{\sqrt{K\varepsilon}}\right)^n - 2u\left(\tau_0 - 2^{\frac{n}{2}}a(n-1)\left(\alpha\frac{u}{\sqrt{K\varepsilon}}\right)^n\right)\frac{\partial\alpha}{\partial u}}\right) \tag{13}$$

For the simpler case of a power-law fluid (τ_0=0), Eq. (14) leads to $\alpha = \frac{\alpha_N}{3}(2+\frac{1}{n})$, which becomes $\alpha = \alpha_N$ for a Newtonian fluid. Therefore, α is a constant parameter only if $\tau_0 = 0$.

Eq. (13) can be numerically solved within a given range of u to obtain the relation between α and u. Then, the obtained relation can be used in Eq. (8) to obtain μ_{eq}. Once μ_{eq} has been determined, it can be entered in Eq. (3), leading to the extension of Darcy's law (Eq. (14)):

$$\nabla P = \frac{\mu_{eq}}{K}u = \frac{C_1}{\alpha} + C_2\alpha^{n-1}u^n \tag{14}$$

with $C_1 = \frac{\tau_0\sqrt{\varepsilon}}{\sqrt{2}\sqrt{K}}$ and $C_2 = \frac{a}{K^{\frac{n+1}{2}}}\left(\frac{2}{\varepsilon}\right)^{\frac{n-1}{2}}$.

It is reminded that the value of α_N is considered first as unknown and must be obtained by fitting Eq. (14) to the experimental (u_i,∇P_i) data. This is achieved by finding the value of α_N that minimizes the sum $E = \sum_{i=1}^{N}(|\nabla P_i - \nabla P(u_i)| \times \nabla P_i)$, with N being the number of experimental data.

By comparing the method presented in this subsection with the works of Chevalier et al. (2013), it can be deduced from Eqs. (2) and (14) that:

$$\chi = \frac{\varepsilon^{\frac{1}{2}}d_s}{2^{\frac{1}{2}}K^{\frac{1}{2}}\alpha} \tag{15}$$

Moreover, Eq. (4) can be used together with Eq. (15) to express χ as a function of only ε and α, obtaining:

$$\chi = \frac{2^{\frac{1}{2}}\kappa^{\frac{1}{2}}3(1-\varepsilon)}{\varepsilon\alpha} = \frac{2^{\frac{1}{2}}5^{\frac{1}{2}}3(1-\varepsilon)}{\varepsilon\alpha} \tag{16}$$

It can be concluded from the preceding equation that χ is a constant at high injection flow rates, given that the value of α is also constant ($\alpha = \alpha^*$). Therefore, the first (yielding) term on the right-hand side of Eq. (2) can be considered a constant at high flow rates. However, this term depends on u at low and moderate values of u, which was not taken into account in the work of Chevalier et al. (2013).

Also, the following relationship can be obtained from comparison between Eqs. (2) and (14):

$$\omega = \frac{2^{\frac{n-1}{2}}}{\varepsilon^{\frac{n-1}{2}}K^{\frac{n+1}{2}}}\alpha^{n-1}d_s^{n+1} \tag{17}$$

Analogously, Eq. (4) can be used together with Eq. (17) to express ω as a function of only ε and α, obtaining:

$$\omega = \frac{2^{\frac{3n+1}{2}}3^{n+1}\kappa^{\frac{n+1}{2}}(1-\varepsilon)^{n+1}}{\varepsilon^{2n+1}}\alpha^{n-1} = \frac{2^{\frac{3n+1}{2}}3^{n+1}5^{\frac{n+1}{2}}(1-\varepsilon)^{n+1}}{\varepsilon^{2n+1}}\alpha^{n-1} \tag{18}$$

Eq. (18) shows that ω is also contant at high flow rates, while being a function of u at moderate and low flow rates. Moreover, ω is not a function of d_s, but depends on the fluid properties through α. This is contrast to the claim of Chevalier et al. (2013) according to which χ and ω are universal factors for a porous medium composed of an assembly of spheres.

It should be kept in mind that elongational flows during the injection of solutions of polymers presenting a certain degree of flexibility through porous media are known to induce extra pressure losses with respect to pure shear flow (Rodríguez et al., 1993; Müller and Sáez, 1999; Nguyen and Kausch, 1999; Seright et al., 2011; Amundarain et al., 2009). This is a result of the formation of transient entanglements of polymer molecules due to the action of the extensional component of the flow. In the present work, we first hypothesize that the deviation of the experimentally measured pressure drop with respect to the viscous pressure drop are negligible. This hypothesis is then validated through analysis of the experimental results.

3. Experimental methods and materials

Experimental ∇P vs. u measurements were performed by injecting a xanthan gum aqueous solution (yield stress fluid) through four packs of spherical glass beads. Flow experiments with filtered water (Newtonian fluid) were also performed by following the procedure presented by Rodríguez de Castro and Radilla (2017a) in order to determine the permeability of the packed beds. The glass beads were first placed into transparent acrylic glass cylinders and then compactly packed by means of vibration with a sieve shaker. The inner diameter of the acrylic glass cylinders was $D = 5$ cm and the diameter of the glass spheres used in each of the four columns was uniform, with ds = 1 mm, 3 mm, 4 mm and 5 mm in each case. The length of the column was $L = 20$ cm.

Two different configurations were used depending on the involved flow rates. For $0.12\,\text{L/h} \le Q \le 6\,\text{L/h}$, the injection circuit was open and the fluid was injected through the packed beds at the selected flow rate using a dual piston pump (Prep Digital HPCL pump, A.I.T., France). For $9\,\text{L/h} \le Q \le 250\,\text{L/h}$, the fluid was injected through a closed circuit using a volumetric pump as performed by Rodríguez de Castro and Radilla (2017a). A photo showing the experimental setup is provided as supplementary material (Fig. S1). Details of the experimental setup and procedure, including the working ranges of the instruments and the measurement uncertainties were provided by Rodríguez de Castro and Radilla (2017a). The ranges of u imposed during the experiments with each packed bed are listed in Table 1.

Xanthan biopolymer is a microbial high molecular weight exopolysaccharide produced by fermentation of X. campestris bacteria (Garcia-Ochoa et al., 2000; Palaniraj and Javarman, 2011; Kumar et al., 2018). In solution state, an isolated macromolecule of this polymer is more or less rigid and with a typical contour length of 1 μm (Mongruel and Cloitre, 2003) and a transverse size of approximately 2 nm. The stiffness of xanthan macromolecules leads to high levels of shear viscosity and highly shear-thinning behaviour of semidilute solutions in water. For this reason, the shear rheology of xanthan gum solutions is well described by the Herschel-Bulkley model (Eq. (1)) under steady-state conditions (García-Ochoa and Casas, 1994; Song et al., 2006; Rodríguez de Castro et al. 2014, 2016, 2018; Rodríguez de Castro and Radilla, 2017b). However, rigorously speaking, they should be referred to as pseudo-yield stress fluids. The capacity of xanthan gum solutions to emulate the shear rheology of a yield stress fluid and the effects of polymer concentration was experimentally assessed by Rodríguez de Castro et al. (2018), concluding that concentrated solutions (~7000 ppm) behave similarly to a yield stress fluid due to high viscosity values at low shear rates.

Sixty litres of aqueous solution were prepared with xanthan gum concentration $C_p = 7000$ ppm and the rheogram was obtained following the procedure presented by Rodríguez de Castro and Radilla (2017b). Eq. (1) was then used to fit the rheogram (Rodríguez de Castro et al., 2014) giving $\tau_0 = 7.4$ Pa, $a = 0.37$ Pa s^n and $n = 0.52$. The rheogram of the solution and the Herschel-Bulkley fit are provided in Fig. 1. The dynamic viscosity of water (solvent) was measured to be 0.0011 Pa s and the densities ρ of both the water and the xanthan gum solution were taken as 1000 kg/m^3. Moreover, the rheograms of several effluent fluid samples were characterized and compared to that of the inflowing fluid at the highest injection flow rates in order to assess polymer degradation and retention on the pore walls. No significant difference was observed between the rheograms, proving that polymer degradation and polymer retention can be neglected.

Despite the used glass beads being quite coarse as compared to most natural granular media, the explored sizes fall within the range of grain sizes reported for coarse sand and fine gravel, which are widely investigated in hydrologic applications (Morris and Johnson, 1967). Moreover, these beads sizes are commonly used in previous research, e.g. Dukhan et al. (2014), so this choice facilitates comparison with literature data. Furthermore, the use of smaller beads may result in polymer retention, which was not observed in the present experiments.

Table 1
Range of average velocities imposed during the flow of the yield stress fluid through the packed beds as a function of d_s. N is the number of experimental ∇P vs. u data (four repetitions for each data).

d_s	Range of u (m/s)	N
1 mm	1.7×10^{-5}–3.5×10^{-3}	27
3 mm	1.7×10^{-5}–3.5×10^{-2}	44
4 mm	1.7×10^{-5}–2.8×10^{-2}	39
5 mm	1.7×10^{-5}–2.8×10^{-2}	33

4. Results

The flow experiments were conducted for both fluids (water and yield stress fluid) and were repeated four times. The number of repetitions for yield stress fluid injection through each packed bed corresponds to $4\times N$ (ranging from 108 to 176) as listed in Table 1. The $4\times N$ measures for each packed bed were considered to be an experimental set. A total of 572 measurements were performed during the flow experiments with the yield stress fluid.

4.1. Experimental determination of ε and k

The weight of each packed bed was measured before and after saturation with water in order to determine ε from the difference in mass. Also, the procedure followed by Rodríguez de Castro and Radilla (2017a) to

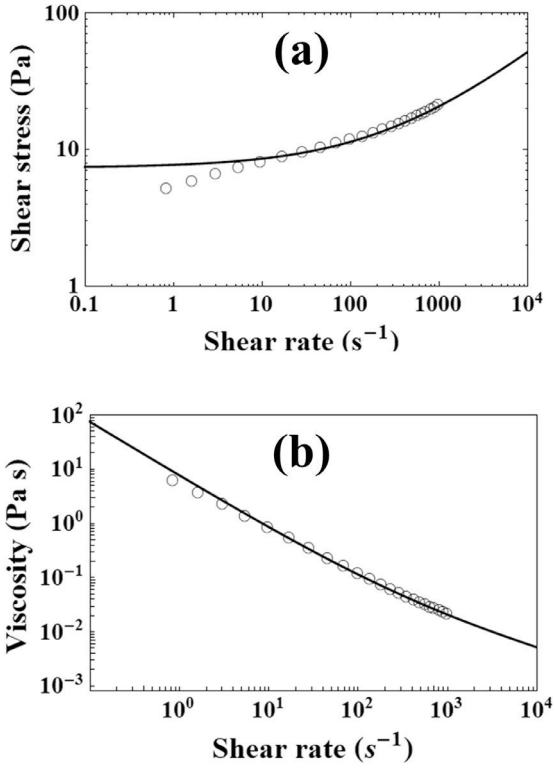

Fig. 1. (a) Rheogram of the injected yield stress fluid and (b) viscosity vs. shear rate relationship. The void circles represent experimental data and black solid lines represent the fitted curves using the Eq. (1).

Table 2
ε and K for the four different beads sizes.

d_s	ε	K
1 mm	0.36 ± 3%	5.9×10^{-10} m^2 ± 2%
3 mm	0.34 ± 3%	5.1×10^{-9} m^2 ± 6%
4 mm	0.35 ± 3%	9.5×10^{-9} m^2 ± 7%
5 mm	0.34 ± 3%	1.3×10^{-8} m^2 ± 6%

Table 3
Values of α_N, α^* and $\hat{\alpha}$ obtained for the four packed beds.

d_s	α_N	α^*	$\hat{\alpha}$
1 mm	0.62	0.81	1.07
3 mm	0.66	0.86	1.01
4 mm	0.63	0.82	1.00
5 mm	0.80	1.04	1.25

determine K from injection experiments with water was applied to the present measurements. The obtained values and for ε and K are listed in Table 2 together with the associated uncertainties (95% confidence interval).

4.2. Shear viscosity of the yield stress fluid in the porous media

Eq. (13) was numerically solved within the involved range of u for both all the investigated packed beds using an implicit Runge-Kutta method. The resulting α versus u functions are represented in Fig. 2 and the results obtained for α_N are listed in Table 3 as a function of d_s. It is noted that the value of α_N was close to 0.68 (average value) in all the tested porous media for the polymer solution used in the present work. This is in very good agreement with the results of Christopher and Middleman (1965), who obtained $\alpha_N = 0.69$.

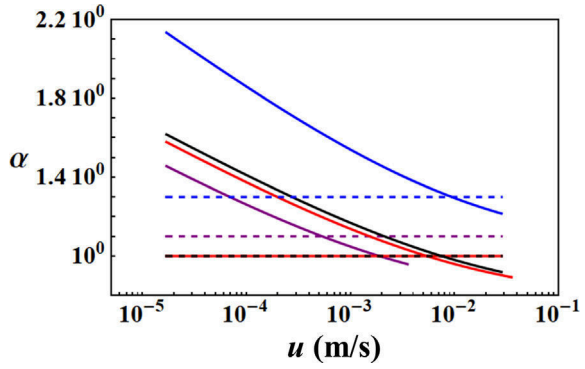

Fig. 2. $\alpha(u)$ functions as numerically obtained from Eq. (13) corresponding to the injection of the 7000-ppm solution through the four packed beds. Purple colour corresponds to $d_s = 1$ mm, red colour corresponds to $d_s = 3$ mm, black colour corresponds to $d_s = 4$ mm and blue colour corresponds to $d_s = 5$ mm. Solid lines represent the computed $\alpha(u)$ functions and dashed lines represent $\hat{\alpha}$.

As mentioned in Section 2.2, α becomes the constant value $\alpha^* = \frac{\alpha_N}{3}(2+\frac{1}{n})$ for very high values of u, i.e., when $u \gg \frac{\tau_0^{\frac{1}{n}} K^{\frac{1}{2}} \varepsilon^{\frac{1}{2}}}{2^{1/2} a^{\frac{1}{n}} \alpha}$, in the case of Herschel-Bulkley shear-thinning fluids ($0 < n < 1$). In Fig. 2, it can be observed that α monotonically decreases as u increases, so the condition $u \gg \frac{\tau_0^{\frac{1}{n}} K^{\frac{1}{2}} \varepsilon^{\frac{1}{2}}}{2^{1/2} a^{\frac{1}{n}} \alpha}$ will be satisfied if $u \gg u^* = \frac{\tau_0^{\frac{1}{n}} K^{\frac{1}{2}} \varepsilon^{\frac{1}{2}}}{2^{1/2} a^{\frac{1}{n}} \alpha^*}$. Consequently, the boundary condition $\alpha\,(u = 10^5\, u^*) = \alpha^*$ was used to numerically solve Eq. (13). The obtained α^* values are also listed in Table 3 and are all close to 0.88 (average value). Regarding the sensitivity of α to the microstructure of the packed bed, it can be deduced from Fig. 2 that higher values of d_s (coarser microstructure) result in higher values of α.

The value of $\dot{\gamma}_{pm}$ corresponding to each Darcy velocity u was calculated with Eq. (7) following two different approaches. First, a constant value of α, named $\hat{\alpha}$ was determined for each porous medium by calculating the shift factor in terms of shear rate which led to the best superposition between the "in situ" μ_{eq} vs. $\dot{\gamma}_{pm}$ data and the bulk rheological law (Eq. (1)). The obtained values for $\hat{\alpha}$ are shown in Table 3. The second approach consisted in using the $\alpha(u)$ function obtained from Eq. (13). The results of both approaches are presented in Fig. 3, together with the bulk rheological law (Eq. (1)). In this figure, it can be observed that μ_{eq} is close to Eq. (1) at high values of u for both the constant α and the variable-α methods. However, this is not the case at low and moderate values of u for which μ_{eq} approaches better Eq. (1) with the variable-α method. Also, μ_{eq} is expected to be greater than the bulk viscosity at high values of u in the presence of important inertial effects (Tosco et al., 2013; Rodríguez de Castro and Radilla, 2016). The fact that no important deviation of μ_{eq} with respect to μ_{pm} is observed in the present experiments reflects that inertial effects are not significant. Moreover, Fig. 3 shows that the shear rates involved in the flow through all porous media are within the same range as those measured with the rheometer during characterization of the fluid's shear viscosity.

4.3. Previous attempts to extend Darcy's law to the flow of yield stress fluids

The values of χ and ω were determined by fitting the experimental results presented in this work to Eq. (2) through minimization of the sum of the absolute values of the differences between fit and experimental data. The obtained values are listed in Table 4, showing that χ and ω are porous medium-dependent as experimentally determined. Also, it is remarked that the values of these coefficients may depend on the range of imposed u, as they are obtained through fitting to experimental data. This dependence on u is taken into account by the new method proposed in the present work, as explained in Section 2.2. The results of fitting Eq. (2) to the experimental data are shown in Fig. 4. Moreover, the

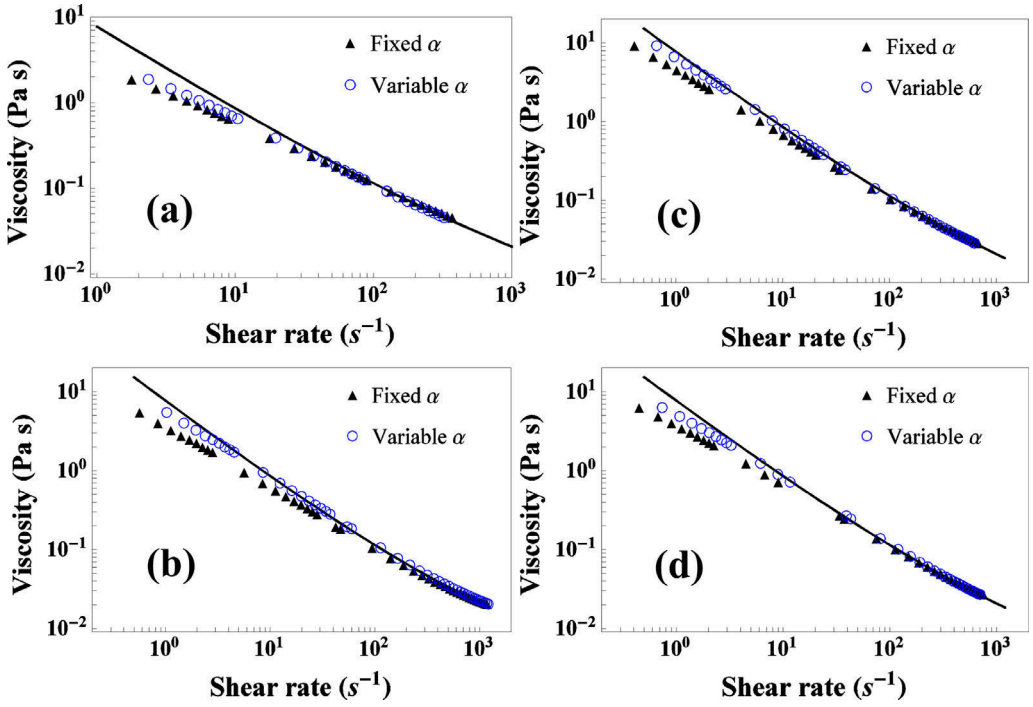

Fig. 3. μ_{eq} for the flow of the yield stress fluids through the four packed beds: (a) $d_s = 1$ mm, (b) $d_s = 3$ mm, (c) $d_s = 4$ mm, (d) $d_s = 5$ mm. Symbols represent predictions and solid lines represent bulk viscosity as obtained from the rheometer (Eq. (1)).

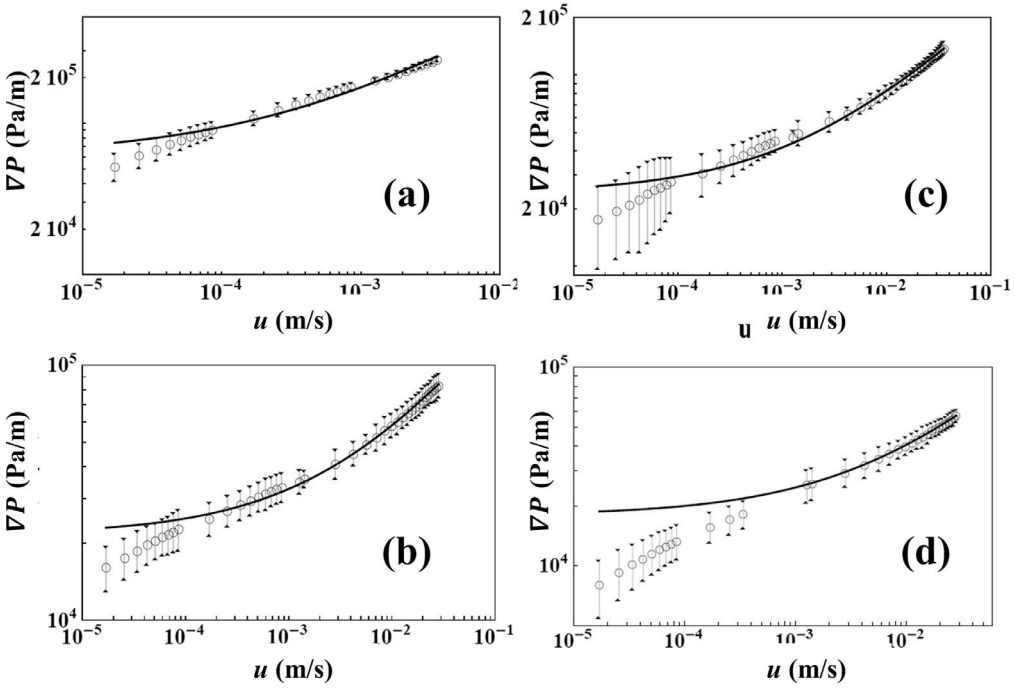

Fig. 4. ∇P as a function of u and the corresponding fits obtained with Eq. (2) for (a) $d_s = 1$ mm, (b) $d_s = 3$ mm, (c) $d_s = 4$ mm, (d) $d_s = 5$ mm.

Table 4
Values of χ and ω used in Eq. (2) for the four packed beds.

d_s	χ	ω
1 mm	8.29	306.32
3 mm	9.86	257.09
4 mm	11.83	247.32
5 mm	12.21	216.82

average errors of these fits are presented in Table 5 for different ranges of u. It is observed that the resulting fits are accurate within a large range of u. However, a major drawback of this method is that χ and ω need to be experimentally determined, which impedes prediction of the u vs. ∇P relation. It is worth mentioning that the errors obtained by using $\chi = 5.5$ and $\omega = 85$ as proposed in the work of Chevalier et al. (2013) are too big in the case of the present experiments and lead to very inaccurate predictions.

Table 5
Average errors obtained by fitting Eq. (2) to the experimental $\nabla \boldsymbol{P}$ vs. u data, with the variable-α method and with the fixed-α method for different ranges of u.

Range of u (m/s)	Average error using Eq. (2) (%)	Average error fixed-α (%)	Average error variable-α (%)
10^{-5}–10^{-4}	32	84	26
10^{-4}–10^{-3}	8	23	5
10^{-3}–10^{-2}	2	7	3
10^{-2}–10^{-1}	1	4	3

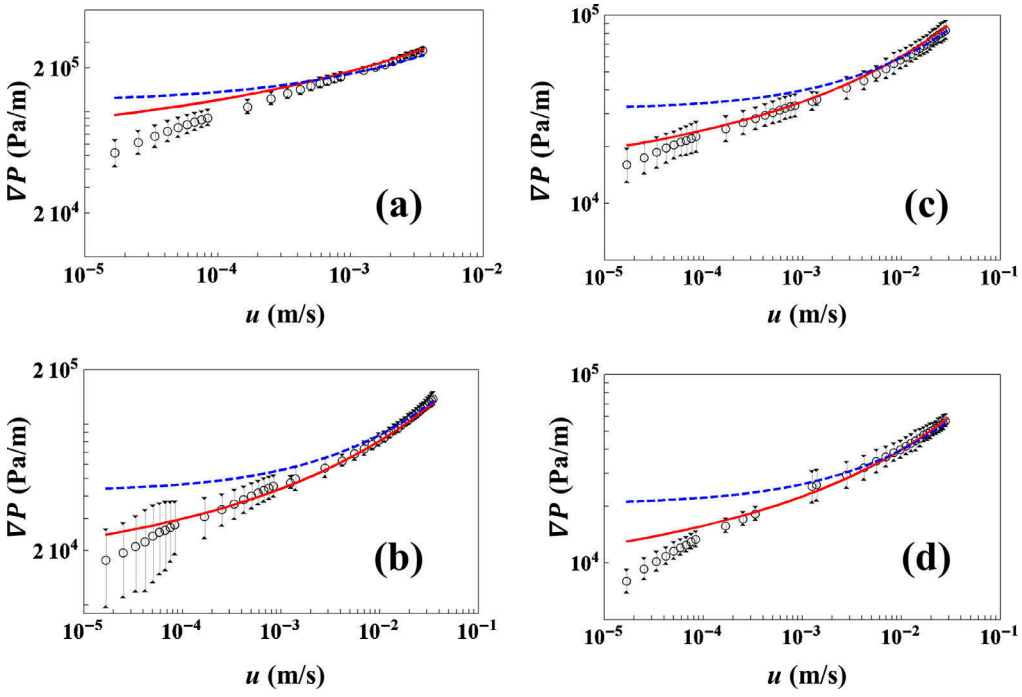

Fig. 5. $\nabla \boldsymbol{P}$ as a function of u and the corresponding predictions obtained with Eq. (14) for (a) $d_s = 1$ mm, (b) $d_s = 3$ mm, (c) $d_s = 4$ mm and (d) $d_s = 5$ mm. Symbols represent experimental measurements, red solid lines represent the predictions obtained with the variable-α method and blue dashed lines represent the predictions obtained with the fixed-α method.

4.4. Experimental validation of the new prediction method

Eq. (14) was used to predict the relation between ∇P and u for the injection of the 7000-ppm solution through the four packed beds. The obtained predictions are presented in Fig. 5 together with the experimental results of measurements performed in the present work. In this figure, the errors bars correspond to a 95% confidence interval as explained in Section 3. From these results, the accuracy of the proposed methods for the prediction of ∇P as a function of u during the flow of yield stress fluids through packed beds of spherical beads can be assessed. Fig. 5 shows that the variable-α approach provides more accurate predictions within the low and moderate u regions, which is in agreement with the arguments presented above. However, a less important difference is obtained between both methods for the highest values of u. The average errors obtained with the variable-α method and the fixed-α method for different ranges of u are summarized in Table 5. It is observed that the variable-α method successfully predicts the ∇P-u relationship for the flow of the yield stress fluid through the four packed beds, even though the obtained predictions are slightly less accurate in the case of $d_s = 1$ mm. The overestimation of ∇P reported in Figs. 4 and 5 for the lowest flow rates may be related to the longer times needed to achieve stationary measurements of pressure drop within this region. This effect is similar as the one reported for rheological measurements at low shear rates, as shown in Fig. 1. This is a consequence of the viscosity of the fluid continuously increasing over time as illustrated in Fig. S2. This effect will be discussed in Section 5."

As mentioned above, α becomes the constant value $\alpha^* = \frac{\alpha_N}{3}(2 + \frac{1}{n})$ when $u \gg u^* = \frac{\tau_0^{\frac{1}{n}} K^{\frac{1}{2}} \varepsilon^{\frac{1}{2}}}{2^{1/2} a^{\frac{1}{n}} \alpha^*}$. This means that Eq. (14) presents a constant yielding term of value $\frac{C_1}{\alpha}$ and a constant "consistency" term of value $C_2 \alpha^{n-1}$ for $u \gg u^*$. In other words, Eq. (14) has the same form as Herschel-Bulkley empirical law (Eq. (1)) only if the preceding condition is met. Therefore, the threshold Reynolds number Re^* above which the extended Darcy's law for Herschel-Bulkley (Eq. (14)) fluids has the same form as Herschel-Bulkley equation is given by:

$$Re^* = \frac{\rho u^* \sqrt{K}}{\mu^*} \tag{19}$$

where μ^* is the shear viscosity of the fluid in the porous media at u^*. Re^* is represented as a function of K for the four packed beds in Fig. 6 showing linear relationship.

It is worth mentioning that, in spite of the negligible influence of inertial effects on the pressure drop vs. flow rate relationships in the case of the highly-viscous xanthan gum solutions used in this work, the procedure presented in Section 2.2. is also valid to extend Forchheimer equation (Forchheimer, 1901) to the case of yield stress fluids. This is explained by the fact that the inertial coefficient appearing in Forchheimer equation does not depend on the shear rheology of the injected fluid as numerically (Firdaouss et al., 1997; Yadzchi and Luding, 2012; Tosco et al., 2013) and experimentally (Rodríguez de Castro and Radilla, 2016; 2017a; 2017b) proved in previous works. However, it must be

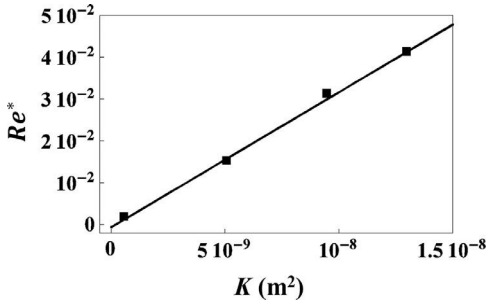

Fig. 6. Threshold Reynolds number $\boldsymbol{Re}^*$ (Eq. (19)) for the injection of the yield stress fluid through the four porous media. Squares represent experimental data and the solid line represents their linear adjustment obtained through standard Least Squares regression: $\boldsymbol{Re}^* = 3.2 \times 10^6\, \boldsymbol{K}(\mathbf{m}^2)$.

noted that even for Newtonian fluids, the macroscopic transport equations governing inertial regime are still under debate in the literature. In particular, it was demonstrated that whereas Forchheimer regime is always well identified for inertial flow in disordered porous media, its appearance in ordered media is strongly dependent on the microstructure and the orientation of the pressure gradient (Lasseux et al., 2011; Agnaou et al., 2017). Therefore, a non-linear dependence of apparent viscosity on pore scale velocity is expected to increase the complexity of the problem.

5. Discussion

The values of α_N obtained for all the tested porous media were always very close to 0.69, which was the value theoretically predicted by (Christopher and Middleman, 1965). It should be noted that although $\alpha_N = 0.69$ is valid for the present experiments, this value must still be confirmed by further experiments in different yield stress fluid-packed beds combinations before declaring that it is a universal constant. Nevertheless, it can be firmly stated that the results reported in this work are a highly promising step in this direction.

It can be deduced from Eq. (14) that α can be considered a constant value $\alpha^* = \frac{\alpha_N}{3}(2+\frac{1}{n})$ in the high flow rates region, i.e., when $u \gg u^* = \frac{\tau_0^{\frac{1}{n}} K^{\frac{1}{2}} \varepsilon^{\frac{1}{2}}}{2^{1/2} a^{\frac{1}{n}} \alpha}$, and Eq. (14) can be written as:

$$\nabla P = \nabla P_0 + C u^n \tag{20}$$

with $\nabla P_0 = \frac{3\tau_0\sqrt{\varepsilon}}{\sqrt{2}\sqrt{K}\alpha_N(2+\frac{1}{n})}$ and $C = \frac{a}{K^{\frac{n+1}{2}}}(\frac{2}{\varepsilon})^{\frac{n-1}{2}}[\frac{\alpha_N}{3}(2+\frac{1}{n})]^{n-1}$. This is in agreement with the results of Talon et al. (2014), who stated that u scales linearly as $(\nabla P - \nabla P_0)$ in the case of a Bingham fluid ($n=1$) flowing at high u through a one-dimensional channel. Also, Nash and Rees (2017) showed that the manner in which flow begins once the threshold pressure gradient is exceeded strongly depends on the channel size distribution of the porous media. The same authors (Talon et al., 2014; Nash and Rees, 2017) proved that ∇P_0 is higher than the actual threshold pressure, which is consistent with our results given that α increases as u tends to zero (Fig. 2).

A model to accurately predict the flow of yield stress and Carreau fluids through rough-walled fractures by using $\alpha_N = 1$ was presented and experimentally validated in a previous work (Rodríguez de Castro and Radilla, 2017b). It is reminded here that α_N is a tortuosity-related factor, so media with different tortuosity may lead to different values of α_N. Indeed, the effective average pore throat radius $\bar{r}_{eff}$, which takes into account the tortuosity of the medium, can be defined as $\bar{r}_{eff} = \sqrt{\frac{8KT}{\varepsilon}} = \bar{r}\sqrt{T} = \frac{\bar{r}}{\alpha_N}$ with $\alpha_N = \frac{1}{\sqrt{T}}$ and T being the tortuosity factor (Christopher and Middleman, 1965; Chaveteau, 1982). Given that the tortuosity of the flow paths in a packed bed is higher than in a fracture, a lower value of α_N is expected for packed beds.

In the case porous media with more complex pore size distributions, the flow is highly conditioned by the narrowest flow paths at low flow rates and the representative pore section should be smaller than $\bar{r}$. In this regard, the full set of equations presented in Section 2.2 should be reconsidered as the current method is not able to capture the influence of pore size distribution. Nevertheless, the use of the present method with more complex porous media should still be useful to predict the relationships between ∇P and u with higher accuracy than the existing methods which use a constant viscosity value.

The existence of yield stress was challenged by Barnes and Walters (1985) and has been discussed for more than 30 years. As explained by Møller et al. (2009), the supporters of the existence of yield stress commonly argue that the viscosity increases very sharply in some materials as the stress decreases towards the yield stress. However, other researchers claim that only a finite and constant viscosity (Newtonian plateau of viscosity) is observed below a certain stress. In particular, Barnes and Walters (1985) used stress-controlled rheometers to show that at low enough shear rates, viscosity reaches a Newtonian plateau for Carbopol and other fluids which had traditionally been considered to have a yield stress. They argued that any material flows providing enough observation time and sufficiently sensitive measuring equipment. In stark contrast with Barnes and Walters (1985) and Møller et al. (2009) experimentally showed that such Newtonian plateau is the consequence of non-steady-state measurements. They demonstrated that for stresses below the yield stress, viscosity is "a priori" unbounded and increases continuously, though slowly, if enough time is allowed. They effectively observed an increase in viscosity even after 100 s. In other words, they found that viscosity is time dependent and tends to infinity below the yield stress. In the case of the present xanthan gum solutions, the evolution of viscosity over time was measured for 1000 s under a shear stress of 0.5 Pa (below the yield stress) using a rheometer equipped with cone/plate geometry. The results are provided as supplementary material (Fig. S2), showing that viscosity does not attain a constant value and continues to increase after that time.

One may wonder whether the proposed procedure is simpler than performing a numerical solution to the actual flow equations, without invoking a bundle-of-capillaries approximation. In this sense, it should be highlighted that performing a numerical solution to the actual flow equations would imply using the size distribution of the flow paths as an input for the model, which is rarely available in real applications. It is reminded that the objective of this work is to present a simple method to predict the pressure drop for the flow of yield stress fluids through packed beds. Therefore, using hardly accessible inputs as needed to perform a numerical solution to the actual flow equations is not a valid approach.

It is noted that in our experiments with yield stress fluids, the total pressure drop through the porous media was successfully predicted from the value of K obtained from water injection without any significant deviation. Therefore, similarly to the case of previous flow experiments with shear-thinning fluids without yield stress (Rodríguez de Castro and Radilla, 2017a), no appreciabe effect of elongational viscosity has been observed in the present work. Also, wall-effect issue during shear-thinning creeping flow in packed beds was previously addressed in the literature. On this subject, Rao and Chhabra (1993) studied the effects of column walls and particle size distribution on the flow rate-pressure drop relationship, proposing a wall correction method and confirming the applicability of the mean hydraulic radius of the particles to characterize a bed of mixed size spheres. The latter authors showed that wall-effect is less significant in the case of shear-thinning fluids than in the Newtonian case. In the present experiments, the porosity of all packed beads is 0.35 ± 0.01 and the experimentally measured permeability is very close to Kozeny-Carman prediction for the largest beads (3.6% difference). Therefore, there is no evidence of significant wall-effect affecting pressure drop vs. flow rate relationship.

A simple approach to extend Darcy's law to the flow of yield stress fluids through packed beds has been presented in this work. This method takes into account the non-proportional relationship between the apparent shear rate in the porous medium $\dot{\gamma}_{pm}$ and average pore velocity u. Only the porosity ε and the permeability K of the porous medium (exclusively for high flow rates) are used as inputs of the method, together with the Herschel-Bulkley parameters of the fluid (τ_0, a, n).

The following procedure to predict ∇P as a function of u is proposed:

(1) Determine the shear-rheology parameters of the fluid using a rheometer: (τ_0, a, n).
(2) Measure the porosity ε of the packed beds, e.g., from difference in mass before and after saturation with water. Note that the usual values are close to $\varepsilon \sim 35\%$.
(3) Measure K from Newtonian-flow experiments. Alternatively, K can be estimated from Kozeny-Carman equation (Eq. (4)) or determined by other techniques (e.g., x-ray tomography). However, the cited methods provide K estimates with very different accuracy, which can be roughly estimated to ~5% for experimental assessment, ~10% for Kozeny-Carman and ~20% for tomography.
(4) Calculate the values of $\alpha(u)$:
  4.1) When low and moderate values of u are involved, solve the following differential equation (Eq. (13)) to obtain $\alpha(u)$:

$$\alpha = \frac{\alpha_N}{\bar{r}} \frac{2\sqrt{2}\sqrt{K}}{3\sqrt{\varepsilon}} \left(2 + \frac{\alpha(\tau_0 + 2^{\frac{n}{2}} a(\alpha \frac{u}{\sqrt{K\varepsilon}})^n)}{2^{\frac{n}{2}} an\alpha(\alpha \frac{u}{\sqrt{K\varepsilon}})^n - 2u(\tau_0 - 2^{\frac{n}{2}} a(n-1)(\alpha \frac{u}{\sqrt{K\varepsilon}})^n) \frac{\partial \alpha}{\partial u}} \right).$$

  A value of $\alpha_N = 0.68$ is proposed, based on the results of the present experiments and previous theoretical works.

  When only high values of u are involved $\left(u \gg u^* = \frac{\tau_0^{\frac{1}{n}} K^{\frac{1}{2}} \varepsilon^{\frac{1}{2}}}{2^{1/2} a^{\frac{1}{n}} \alpha^*} \right)$, use a constant value $\alpha = \alpha^* = \frac{\alpha_N}{3}(2 + \frac{1}{n})$.
  4.2) Use Eq. (8) to compute μ_{eq} as a function of u, ε, K, τ_0, a and n:

$$\mu_{eq} = \frac{\tau_0 \sqrt{K\varepsilon}}{\alpha\sqrt{2}u} + a\left(\alpha \frac{\sqrt{2}u}{\sqrt{K\varepsilon}} \right)^{n-1}$$

(5) Use Eq. (14) to calculate ∇P as a function of u:

$$\nabla P = \frac{\mu_{eq}}{K} u = \frac{C_1}{\alpha} + C_2 \alpha^{n-1} u^n$$

with $C_1 = \frac{\tau_0 \sqrt{\varepsilon}}{\sqrt{2}\sqrt{K}}$ and $C_2 = \frac{a}{K^{\frac{n+1}{2}}} \left(\frac{2}{\varepsilon} \right)^{\frac{n-1}{2}}$.

Flow experiments of yield stress fluids covering a wide range of u were performed in order to assess the accuracy of the predictions obtained using the proposed method, showing good agreement between model and experiments and negligible inertial effects within the explored range of u. Consequently, Darcy's law provides accurate u-∇P predictions in contrast to the case of less concentrated solutions with no yield stress in which inertial effects were significant (Rodríguez de Castro and Radilla, 2017a).

As an important industrial application, the extended Darcy's law can be included in computational studies of large-scale non-Newtonian flow in unconsolidated porous media. The conclusions of this work have now to be assessed using real granular media. Also, future numerical studies should be performed in order to provide deeper insight into the physical mechanisms governing the non-proportional relationship between $\dot{\gamma}_{pm}$ and u.

Acknowledgments

The author would like to acknowledge Pr. Giovanni Radilla for providing the equipment used in the experimental part of this work. The author also wishes to thank Frédéric Bastien for his technical support throughout the experimental campaign.

Supplementary material associated with this article can be found, in the online version, at doi:10.1016/j.advwatres.2019.01.012.

References

Agnaou, M., Lasseux, D., Ahmadi, A., 2017. Origin of the inertial deviation from Darcy's law: an investigation from a microscopic flow analysis on two-dimensional model structures. Phys. Rev. E 96, 043105.
Al-Fariss, T., Pinder, K.L., 1987. Flow through porous media of a shear-thinning liquid with yield stress. Can. J. Chem. Eng. 65, 391–405.
Amundarain, J.L., Castro, L.J., Rojas, M.R., Siquier, S., Ramírez, N., Müller, A.J., Sáez, A.E., 2009. Solutions of xanthan gum/guar gum mixtures: shear rheology, porous media flow, and solids transport in annular flow. Rheol. Acta 48, 491–498.
Barnes, H., Walters, K., 1985. The yield stress myth? Rheol. Acta 24, 323–326.
Basu, S., 2001. Wall effect in laminar flow of non-Newtonian fluid through a packed bed. Chem. Eng. J. 81, 323–329.
Belyadi, H., Fathi, E., Belyadi, F., 2016. Hydraulic Fracturing in Unconventional Reservoirs. Theories, Operation,s and Economics Analysis, First Edition Gulf Professional Publishing, Elsevier Ch. 8.
Benmouffok-Benbelkacem, G., Caton, F., Baravian, C., Skali-Lami, S., 2010. Non-linear viscoelasticity and temporal behavior of typical yield stress fluids. Carbopol, Xanthan and Ketchup. Rheol. Acta 49, 305–314.
Carnali, J.O., 1991. A dispersed anisotropic phase as the origin of the weak-gel properties of aqueous xanthan gum. J. Appl. Polymer Sci. 43 (5), 929–941.
Chauveteau, G., 1982. Rodlike polymer solution flow through fine pores: influence of pore size on Rheological behavior. J. Rheol. 26, 111.
Chauveteau, G., Zaitoun, A., 1981. Basic Rheological behavior of Xanthan polysaccharide solutions in porous media: effects of pore size and polymer concentration. European Symposium on Enhanced Oil Recovery.
Chase, G., Dachavijit, P.A, 2005. Correlation for yield stress fluid flow through packed beds. Rheol. Acta 44, 495–501.
Chevalier, T., Chevalier, C., Clain, X., Dupla, J.C., Canou, J., Rodts, S., Coussot, P., 2013. Darcy's law for yield stress fluid flowing through a porous medium. J. Non-Newton. Fluid Mech. 195, 57–66.
Chevalier, T., Rodts, S., Chateau, X., Chevalier, C., Coussot, P., 2014. Breaking of non-Newtonian character in flows through a porous medium. Phys. Rev. E 89, 023002.
Chhabra, R.P., Comiti, J., Machac, I., 2001. Flow of non-Newtonian fluids in fixed and fluidised beds. Chem. Eng. Sci. 56, 1–27.
Christopher, R.H., Middleman, S., 1965. Power-law flow through a packed tube. Ind. Eng. Chem. Fundament. 4 (4), 422–426. https://doi.org/10.1021/i160016a011.
Comba, S., Dalmazzo, D., Santagata, E., Sethi, R., 2011. Rheological characterization of xanthan suspensions of nanoscale iron for injection in porous media. J. Hazardous Mater. 185, 598–605.
Coussot, P., 2014. Yield stress fluid flows: A review of experimental data. J. Non-Newton. Fluid Mech. 211, 31–49.
Darcy, H.P.G., 1856. Les Fontaines Publiques De La Ville De Dijon. Libraire des Corps Imperiaux des Ponts et Chaussées et des Mines, Paris, pp. 590–594.
Dukhan, N., Bağcı, Ö., Özdemir, M., 2014. Experimental flow in various porous media and reconciliation of Forchheimer and Ergun relations. Exp. Thermal Fluid Sci. 57, 425–433. https://doi.org/10.1016/j.expthermflusci.2014.06.011.
Economides, M.J., Nolte, K.G., 2000. Reservoir Stimulation, Third edition Wiley, New York.
Firdaouss, M., Guermond, J.-L., Le-quéré, P., 1997. Nonlinear correction to Darcy's law at low Reynolds numbers. J. Fluid Mech. 343, 331–350. https://doi.org/10.1017/S0022112097005843.
Forchheimer, P., 1901. Wasserberwegng durch Boden. Forschtlft ver. D. Ing. 45 (50), 1782–1788.
García-Ochoa, F., Casas, J.A., 1994. Apparent yield stress in xanthan gum solutions at low concentrations. Chem. Eng. J. 53, B41–B46.
García-Ochoa, F., Santosa, V.E., Casasb, J.A., Gómez, E., 2000. Xanthan gum: production, recovery, and properties. Biotechnol. Adv. 18, 549–579.
Gastone, F., T., Tosco, Rajandrea, S., 2014. Green stabilization of microscale iron particles using guar gum: Bulk rheology, sedimentation rate and enzymatic degradation. J. Colloid Interface Sci. 421, 33–43.
Herschel, W.H., Bulkley, R., 1926. Konsistenzmessungen von Gummi-Benzollösungen. Kolloid-Zeitschrift 39, 291. https://doi.org/10.1007/BF01432034.
James, D.F., McLaren, D.R., 1975. The laminar flow of dilute polymer solutions through porous media. J. Fluid Mech. 70 (4), 733–752. https://doi.org/10.1017/S0022112075002327.
Kaviany, M., 1995. Principles of Heat Transfer in Porous Media. Springer, New York, p. 3. Ch.2.
Khodja, M., 2008. Les Fluides de forage: étude des Performances et Considerations Environnementales PhD thesis. Institut National Polytechnique de Toulouse.
Kozeny, J., 1927. Ueber kapillare Leitung des Wassers im Boden. Sitzungsber Akad. Wiss., Wien 136 (2a), 271–306.
Kumar, A., Rao, K.M., Han, S.S., 2018. Application of xanthan gum as polysaccharide in tissue engineering: a review. Carbohydr. Polym. 180, 128–144.
Lasseux, D., Abbasian Arani, A.A., Ahmadi, A., 2011. On the stationary macroscopic inertial effects for one phase flow in ordered and disordered porous media. Phys. Fluids 23, 073103. https://doi.org/10.1063/1.3615514.
Lavrov, A., 2013. Non-Newtonian fluid flow in rough-walled fractures: a brief review. In: Proceedings of ISRM SINOROCK 2013, 18-20 June. Shanghai, China.

Lake, LW., 1989. Enhanced Oil Recovery. Prentice-Hall Inc, Englewood Cliffs, NJ.
López, X., Valvatne, P.H., Blunt, M.J., 2003. Predictive network modeling of single-phase non-Newtonian flow in porous media. J. Colloid Interface Sci. 264 (1), 256–265. https://doi.org/10.1016/s0021-9797(03)00310-2.
López, X., 2004. Department of Earth Science & Engineering Petroleum Engineering & Rock Mechanics Group PhD Thesis. Imperial College, London.
Macosko, C.W., 1994. Rheology: principles, Measurements and Applications. Wiley-VCH.
Møller, P.C.F., Fall, A., Bonn, D., 2009. Origin of apparent viscosity in yield stress fluids below yielding. Europhys. Lett. Assoc. 87 (3).
Mongruel, A., Cloitre, M., 2003. Axisymmetric orifice flow for measuring the elongational viscosity of semi-rigid polymer solutions. J. non-Newt. Fluid Mech. 110, 27–43.
Mooney, M.J., 1931. Explicit formulas for slip and fluidity. J. Rheol. 2, 210–222.
Morris, D.A., Johnson, A.I., 1967. Summary of hydrologic and physical properties of rock and soil materials, as analyzed by the hydrologic laboratory of US geological survey 1948–60. In: Water Supply Paper 1839-D, US Geological Survey, Washington, p. 42.
Müller, A.J., Sáez, A.E., 1999. The rheology of polymer solutions in porous media. In: Nguyen, T.Q., Kausch, H.H. (Eds.), Flexible Polymer Chain Dynamics in Elongational flow: Theory and Experiment. Springer, Heidelberg, pp. 335–393.
Nash, S., Rees, D.A.S., 2017. The effect of microstructure on models for the flow of a Bingham fluid in porous media: one-dimensional flows. Transport Porous Med. 116 (3), 1073–1092. https://doi.org/10.1007/s11242-016-0813-9.
Nguyen, T.Q., Kausch, H.H., 1999. Flexible Polymer Chains in Elongational Flow: Theory and Experiement. Springer, Berlin.
Palaniraj, A., Jayaraman, V., 2011. Production, recovery and applications of xanthan gum by Xanthomonas campestris. J. Food Eng. 106, 1–12.
Pang, Z., Liu, H., 2013. The study on permeability reduction during steam injection in unconsolidated porous media. J. Petroleum Sci. Eng. 106, 77–84. https://doi.org/10.1016/j.petrol.2013.04.022.
Pascal, H., 1981. Nonsteady flow through porous media in the presence of a threshold gradient. Acta Mech. 39, 207–224. https://doi.org/10.1007/BF01170343.
Peng, S., Fu, J., Zhang, J., 2007. Borehole casing failure analysis in unconsolidated formations: a case study. J. Petroleum Sci. Eng. 59, 226–238.
Pipe, C.J., Majmudar, T.S., McKinley, G.H., 2008. High shear rate viscometry. Rheol. Acta 47, 621–642. https://doi.org/10.1007/s00397-008-0268-1.
Rabinowitsch, B., 1929. Ueber die viskositat und elastizitat von solen. Z Physik Chem. Ser. A 145, 1–26.
Rao, P.T., Chhabra, R.P., 1993. Viscous non-Newtonian flow in packed beads: effects of column walls and particle size distribution. Powder Technol. 77, 171–176.
Rodríguez, S., Romero, C., Sargenti, M.L., Müller, A.J., Sáez, A.E., Odell, J.A., 1993. Flow of polymer solutions through porous media. J. Non-Newt. Fluid Mech. 49, 63–85.
Rodríguez de Castro, A., 2014. Flow Experiments of Yield Stress Fluids in Porous Media as a New Porosimetry Method PhD thesis. Arts et Métiers ParisTech.
Rodríguez de Castro, A., Omari, A., Ahmadi-Sénichault, A., Bruneau, D., 2014. Toward a new method of porosimetry: principles and experiments. Transport Porous Med. 101 (3), 349–364. https://doi.org/10.1007/s11242-013-0248-5.
Rodríguez de Castro, A., Omari, A., Ahmadi-Sénichault, A., Savin, S., Madariaga, L.-F., 2016. Characterizing porous media with the yield stress fluids porosimetry method. Transport Porous Med. 114 (1), 213–233. https://doi.org/10.1007/s11242-016-0734-7.
Rodríguez de Castro, A., Ahmadi-Sénichault, A., Omari, A., 2018. Using Xanthan Gum solutions to characterize porous media with the yield stress fluids porosimetry method: robustness of the method and effects of polymer concentration. Transport Porous Med. 122 (2), 357–374. https://doi.org/10.1007/s11242-018-1011-8.
Rodríguez de Castro, A., Radilla, G., 2016. Non-Darcian flow experiments of shear-thinning fluids through rough-walled rock fractures. Water Resour. Res. 52 (11), 9020–9035. https://doi.org/10.1002/2016WR019406.
Rodríguez de Castro, A., Radilla, G., 2017a. Non-Darcian flow of shear-thinning fluids through packed beads: experiments and predictions using Forchheimer's law and Ergun's equation. Adv. Water Resour. 100, 35–47. https://doi.org/10.1016/j.advwatres.2016.12.009.
Rodríguez de Castro, A., Radilla, G., 2017b. Flow of yield and Carreau fluids through rough-walled rock fractures: prediction and experiments. Water Resour. Res. 53 (7), 6197–6217. https://doi.org/10.1002/2017WR020520.
Roustaei, A., Chevalier, T., Talon, L., Frigaard, I.A., 2016. Non-Darcy effects in fracture flows of a yield stress fluid. J. Fluid Mech. 805, 222–261. https://doi.org/10.1017/jfm.2016.491.
Seright, R.S., Fan, T., Wavrik, K., de Carvalho Balaban, R., 2011. New Insights into polymer rheology in porous media. SPE J. 16. https://doi.org/10.2118/129200-PA.
Shahsavari, S., McKinley, G.H., 2016. Mobility and pore-scale fluid dynamics of rate-dependent yield-stress fluids flowing through fibrous porous media. J. Non-Newt. Fluid Mech. 235, 76–82.
Sheng, J.J., 2011. Modern Chemical Enhanced Oil Recovery, Theory and Practice. GPG. Elsevier, Boston.
Shenoy, A.V., 1994. Non-Newtonian Fluid Heat transfer in porous media. Adv. Heat Transfer 24, 101–190. https://doi.org/10.1016/S0065-2717(08)70233-8.
Silva, J.A.K., Smith, M., Munakata-Marr, J., McCray, J.E., 2012. The effect of system variables on In situ sweep-efficiency improvement via viscosity modification. J. Contam. Hydrol. 136, 117–130.
Sochi, T., 2010. Non-Newtonian flow in porous media. Polymer 51, 5007–5023.
Sochi, T., 2015. Analytical solutions for the flow of Carreau and cross fluids in circular pipes and thin slits. Rheol. Acta 48, 491–498.
Song, K.-W., Kim, Y.–S., Chang, G.S., 2006. Rheology of concentrated xanthan gum solutions: steady shear flow behavior. Fiber. Polym. 7 (2), 129–138.
Sorbie, K.S., Clifford, P.J., Jones, R.W., 1989. The rheology of pseudoplastic fluids in porous media using network modeling. J. Colloid Interface Sci. 130, 508–534.
Steffe, J.F., 1996. Rheological Methods in Food Process Engineering, Second Edition Freeman Press, East Lansing Ch. 2.
Talon, L., Auradou, H., Hansen, A., 2014. Effective rheology of Bingham fluids in a rough channel. Front. Phys. 2, 24. https://doi.org/10.3389/fphy.2014.00024.
Talon, L., Bauer, D., 2013. On the determination of a generalized Darcy equation for yield-stress fluid in porous media using a Lattice-Boltzmann TRT scheme. Eur. Phys. J. E 36, 1–10.
Tiu, C., Zhou, J.Z.Q., Nicolae, G., Fang, T.N., Chhabra, R.P., 1997. Flow of viscoelastic polymer solutions in mixed beds of particles. Canadian J. Chem. Eng. 75, 843–850.
Tosco, T., Marchisio, D.L., Lince, F., Sethi, R., 2013. Extension of the Darcy–Forchheimer law for shear-thinning fluids and validation via pore-scale flow simulations. Transport Porous Med. 96, 1–20. https://doi.org/10.1007/s11242-012-0070-5.
Wang, L., Tian, Y., Yu, X., Wang, C., Yao, B., Wang, S., Winterfeld, P.H., Wang, X., Yang, Z., Wang, Y., Cui, J., Wu, Y.-S., 2017. Advances in improved/enhanced oil recovery technologies for tight and shale reservoirs. Fuel 210, 425–445.
Welti-Chanes, J., Vergara-Balderas, F., Bermúdez-Aguirre, D., 2005. Transport phenomena in food engineering: basic concepts and advances. J. Food Eng. 67, 113–128.
Wever, D.A.Z., Picchioni, F., Broekhuis, A.A., 2011. Polymers for enhanced oil recovery: a paradigm for structure–property relationship in aqueous solution. Progress Polymer Sci. 36 (11), 1558–1628.
Withcomb, P.J., Macosko, C.W., 1978. Rheology of xanthan gum. J. Rheol. 22, 493.
Yazdchi, K., Luding, S., 2012. Towards unified drag laws for inertial flow through fibrous materials. Chem. Eng. J. 207-208, 35–48.